Chapter I

Introduction

Due to the properties of low loss, reliable and durable, rectangular waveguide, one of the traditional transmission lines, is widely used in military and deep-space communication systems. However, rectangular waveguide are not compact, expensive to manufacture, and difficult to be integrated with planar circuits [1]-[4]. In addition to the application of signal transmission using metallic waveguide, it can be employed to design a filter, which is named as waveguide filter. However, a high precision mechanical process and a fine tuning mechanism are needed to obtain high-performance filters. Recently, a new structure of printed waveguide technique, which is so-called the Substrate Integrated Waveguide (SIW) has been developed to meet these requirements [5]-[6], and a number of components have been studied and implemented at microwave/millimeter frequencies [7].

Substrate Integrated Waveguide (SIW) technology presents a new design scheme employing the via-holes array or post-wall to mimic the waveguide side walls for reflecting the incident wave. Since it is based on the printed circuit board process, it can be integrated with the planar transmission lines, such as co-planar waveguide or micro-strip, and the passive components.

Since the electromagnetic field distribution in SIW is similar to that in a conventional rectangular waveguide, it may inherent the advantages of a metallic waveguide. Hongjun Tang *et al.* [8] developed a Sub-harmonic Mixer with a high-Q SIW resonator. SIW linear phase filter have been designed by Xiaoping Chen *et al.* [9].

Since the communication systems using multiple bandwidths become dominant, the passive-, active- component and antennas operated in multiple bandwidths gradually attract considerable attentions. For instance, dual-bandpass and multi-band components, including

antennas [10], amplifiers [11], and microwave filters [12]-[13], become key components in these communications systems and have been studied previously. A number of publications have been provided a variety of solutions to realize dual-bandpass filters. Tsai and Hsue [14] inserted a stop-band into a broadband to form dual- bandpass by cascading a broadband filter with a narrowband band-stop filter. Miyake *et al.*[15] used two different parallel-connected filters to obtain dual-bandpass filter.

The operation mechanisms of diplexer and dual-bandpass filter are similar to each other. However, the major difference between these two structures is that a diplexer configuration divides the signal into two paths, while the dual-bandpass filter has only one signal path.

In this thesis, we propose a new dual-bandpass SIW filter. The proposed filter is composed of two waveguides and two cavities implemented using via-holes array technology. Because of the bend structure was employed, this dual-bandpass filter can achieve a good rejection for the higher harmonics.

The organization of this thesis is given as follow. Chapter Ⅱ introduces the structure configuration and the fabrication process of the filter under consideration. Chapter Ⅲ demonstrates the numerical and experimental results, and briefly discusses the physical phenomenon associated with the electric field distribution within the structure. In chapter IV, we will give some remarks to conclude this chapter.

Chapter Ⅱ

Structure configuration and fabrication process

Via-holes array waveguide

As shown in figure 1, a via-holes array waveguide consists of top and bottom metal plates separated by a low-loss dielectric substrate. The via-holes arrays were employed to serve as the waveguide side walls to reflect the incident wave. Therefore, the wave is bouncing back and forth and is propagating along the waveguide axis. It is noted that due to the existence of loss tangent with the dielectric substrate this waveguide may have considerable dielectric loss compared with the commonly used metallic waveguide filled with air. Besides, from the reports of the literature [K. Wu], the pitch between the adjacent via holes has to be carefully designed to avoid the electromagnetic wave leakage.

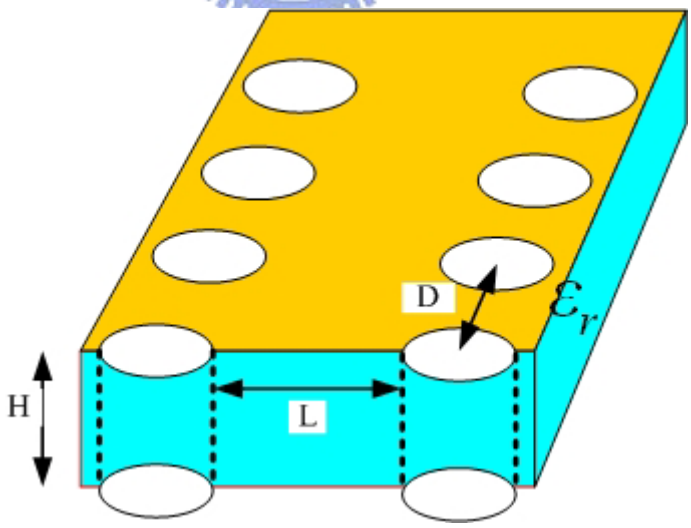

Figure 1. Structure configuration of via-holes array waveguide

Dual-bandpass filter

The structure configuration for the proposed dual-bandpass filter is shown in Figure 2. This

filter includes two micro-strip transitions, two SIW cavities and two SIW waveguides. The wave propagating region is within the two arrays of via holes. In this filter, the SIW cavities are coupled to each other in the H-plane. The excitation of the waveguide is through the micro-strip line with linear taper transition to achieve the impedance match between micro-strip line and rectangular waveguide. Here, the taper micro-strip is used to transform the quasi-TEM mode of the micro-strip line into the TE_{10} mode in the rectangular waveguide. For all of the examples discussed in this thesis, the design procedure was given as follows. The first step is to design the dimensions of a SIW cavity at the desired frequency. In view of the pass band frequencies are caused by the resonance of the cavities, the resonant frequency of a cavity mode with indices pair *(m, n)* can be roughly determined by the formula given below

$$f_{TE_{mno}}(\text{in GH z}) = \frac{150}{\sqrt{\varepsilon_s}}\sqrt{(\frac{m}{l})^2 + (\frac{n}{w})^2}$$

Parameters l and w are the length and the width of cavity. Parameter ε_s is the relative dielectric constant of the dielectric substrate. The integer *m*, *n* and *o* denote the index number along the three directions. Although the exact formula for the pass band frequencies can not be obtained in this research, the tendency of variation for the structure parameters were observed carefully and summarized in the flowing paragraph.

(1) the second pass-band frequency is swinging as the cavity length l is changing (w is fixed)

(2) the pass-band bandwidth relates to the parameter w_a, the width of aperture; the wider the parameter w_a, the wider the pass-band bandwidth

(3) this filter can be designed and fine tuned by using an efficient full-wave simulator.

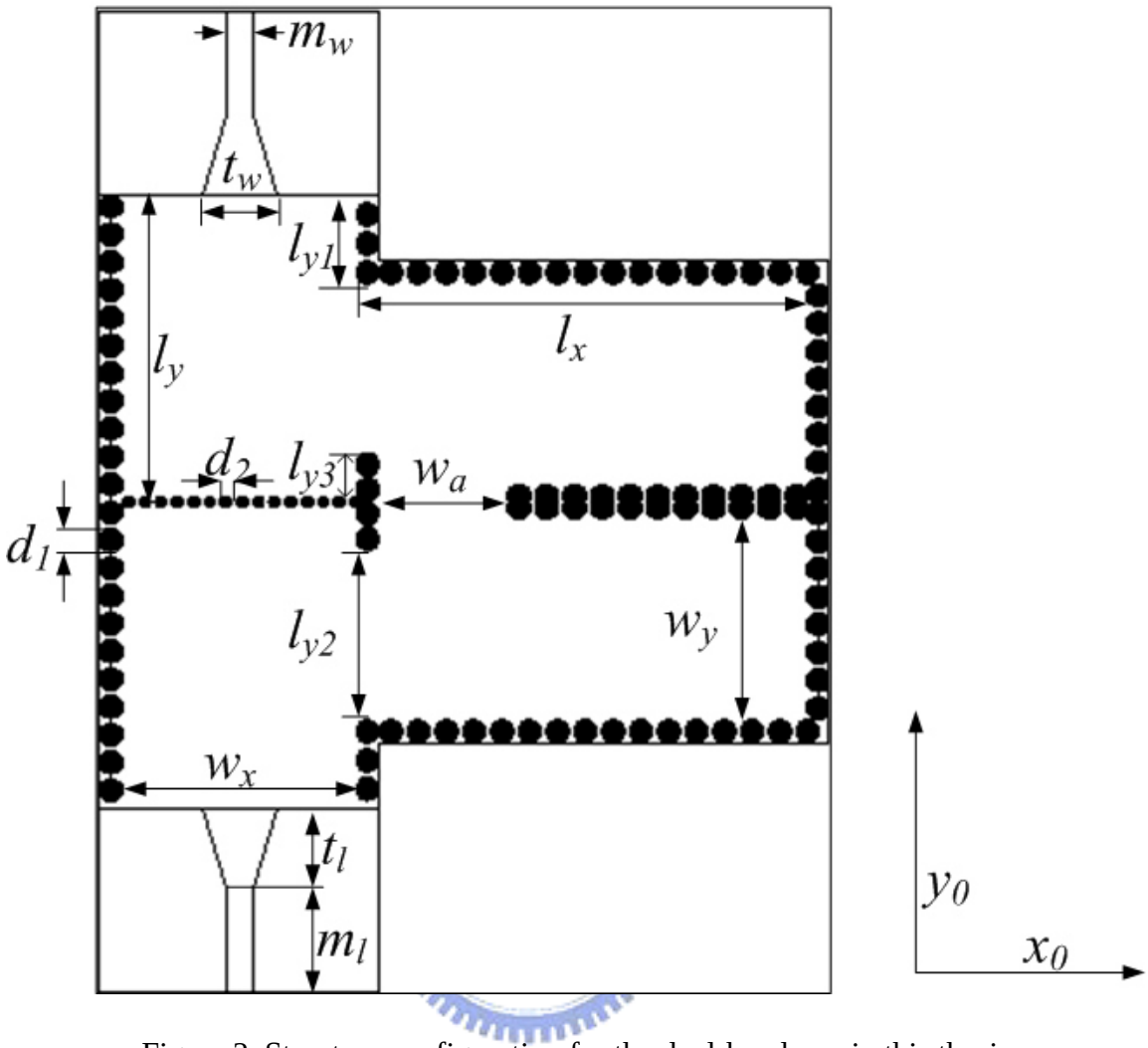

Figure 2. Structure configuration for the dual-bandpass in this thesis

Chapter Ⅲ

The numerical and experimental results

Due to the presence of higher harmonics response, it constitutes a well-known problem for most of the dual-bandpass filters. This problem can result in poor harmonic signal suppression when the filters are used as output components. Therefore, a technique to eliminate these unwanted responses in filters is required. Although the higher harmonics suppression in band-pass filters has been an object of study for a long time, only few studies so far have been made at the higher harmonics suppression in dual-bandpass filters.

To show the improved stop-band characteristics of the proposed filters, we designed the two dual-bandpass filters with the same structure parameters. One of them is designed to the input/output substrate integrated waveguide which are the same side and directly connected with the cavities, as shown in figure 3. The other is designed to the input/output substrate integrated waveguide which are turned 90 degree and connected with the cavity, as shown in Figure 4. The first and the second pass band frequencies of these filters are designed at 9.17 GHz and 10.2 GHz, respectively. Figure 5 shows the simulated results by comparing the two filters with different the input/output design structures. As can be seen from figure 5, the filters with bend design can suppress the higher harmonics from 11.2 to 15.5 GHz and a rejection level around 25dB, while the higher harmonics of the filter without bend design start at 12.4GHz and 14.9 GHz. In other words, the proposed dual-bandpass filter with bend design has relatively wide and deep stop-band characteristics.

To explain this rejection from 11.2 to 15.5 GHz is due to the input/output substrate integrated waveguide bend design, the simulated electric field strength (E_z) distribution on the cross section at half thickness of the substrate over each cavity is plotted in figure 6 (a)-(d).

Firstly, figure 6 (a) and 6 (b) show the electric field strength (E_z) distribution of the filters

with bend design and without bend design at 9.1 GHz and 10.2 GHz, respectively. These figures indicate that the two filters with distinct input/output substrate integrated waveguide bend design have the same resonant mode,TE_{110} and TE_{210}, to produce the first and the second pass band response .

Secondly, the electric field strength (E_z) distribution of the filter without bend design at 12.4 GHz and 14.8 GHz are shown in figure 6 (c). Due to the higher order resonances produced by the resonant mode, TE_{310} and TE_{410} , the filter without bend design has quite strong electromagnetic field from the cavity 1 coupled to the cavity 2 through a aperture. Therefore, there are higher harmonics to appear around 12.4 GHz and 14.76 GHz.

Finally, the electric field strength (E_z) distribution of the filter with bend design at 12.4 GHz and 14.8 GHz are shown in figure 6 (d). However, comparing figure 6 (b) with figure 6 (c), it is obvious that there is a weak electric field strength (E_z) within the cavity 4. Thus the filter with the input/output substrate integrated waveguide bend design can block the most of electromagnetic field from the cavity 3 coupled to the cavity 4 at 12.4 GHz and 14.76 GHz.

From the above a series of four figures illustrate if the input/output substrate integrated waveguide are turned 90 degree to connect the cavity, the higher harmonics responses are suppressed effectively. Thus the proposed dual-bandpass filter with bend design can provide the ability of higher harmonic suppression .

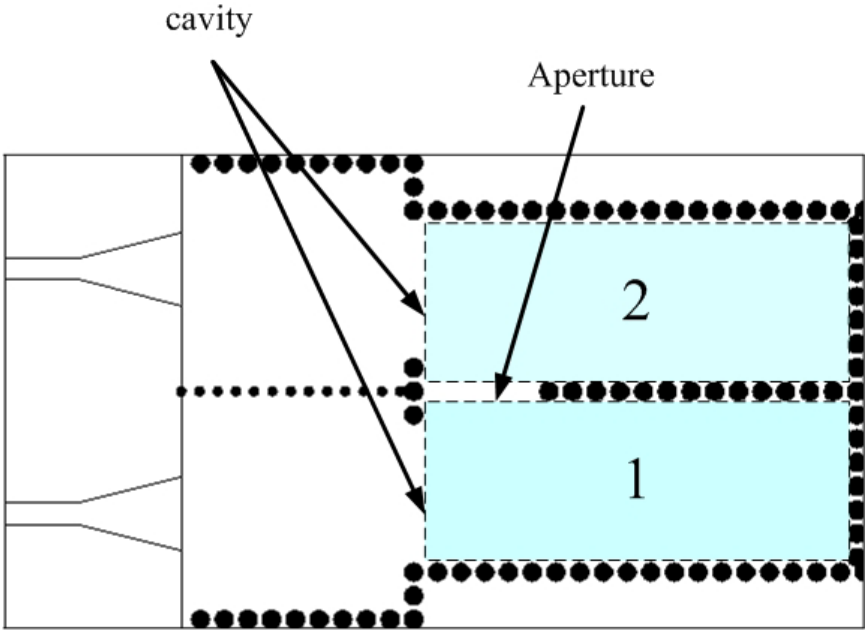

Figure 3. Configuration of the filter which the input/output substrate integrated waveguide is directly connected with the cavities

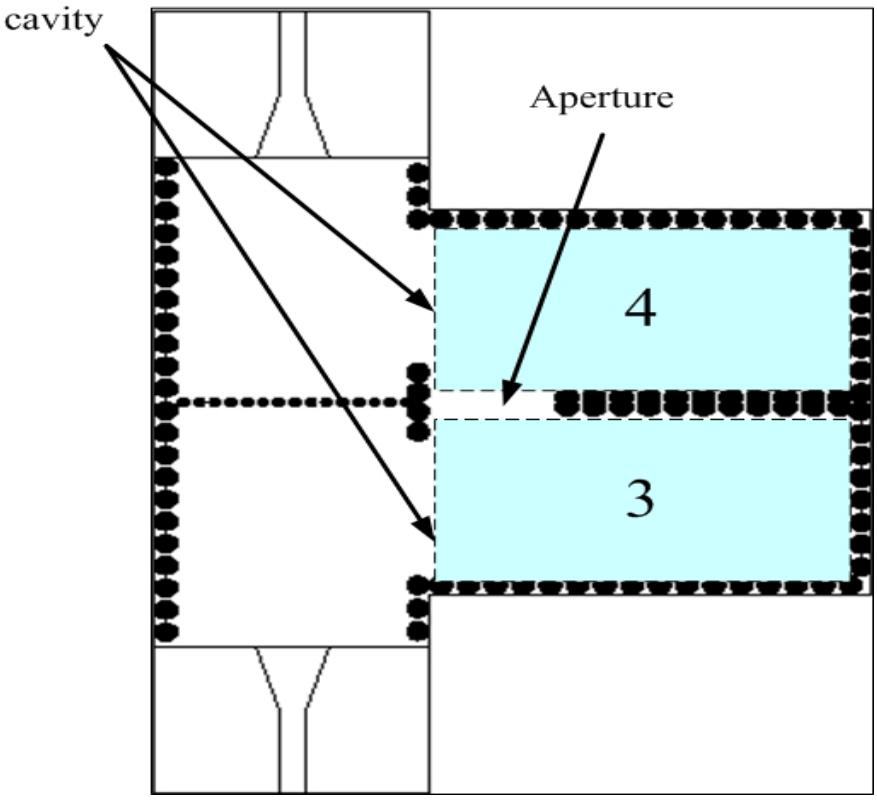

Figure 4. Configuration of the filter which the input/output substrate integrated waveguide is turned 90 degree and connected with the cavities

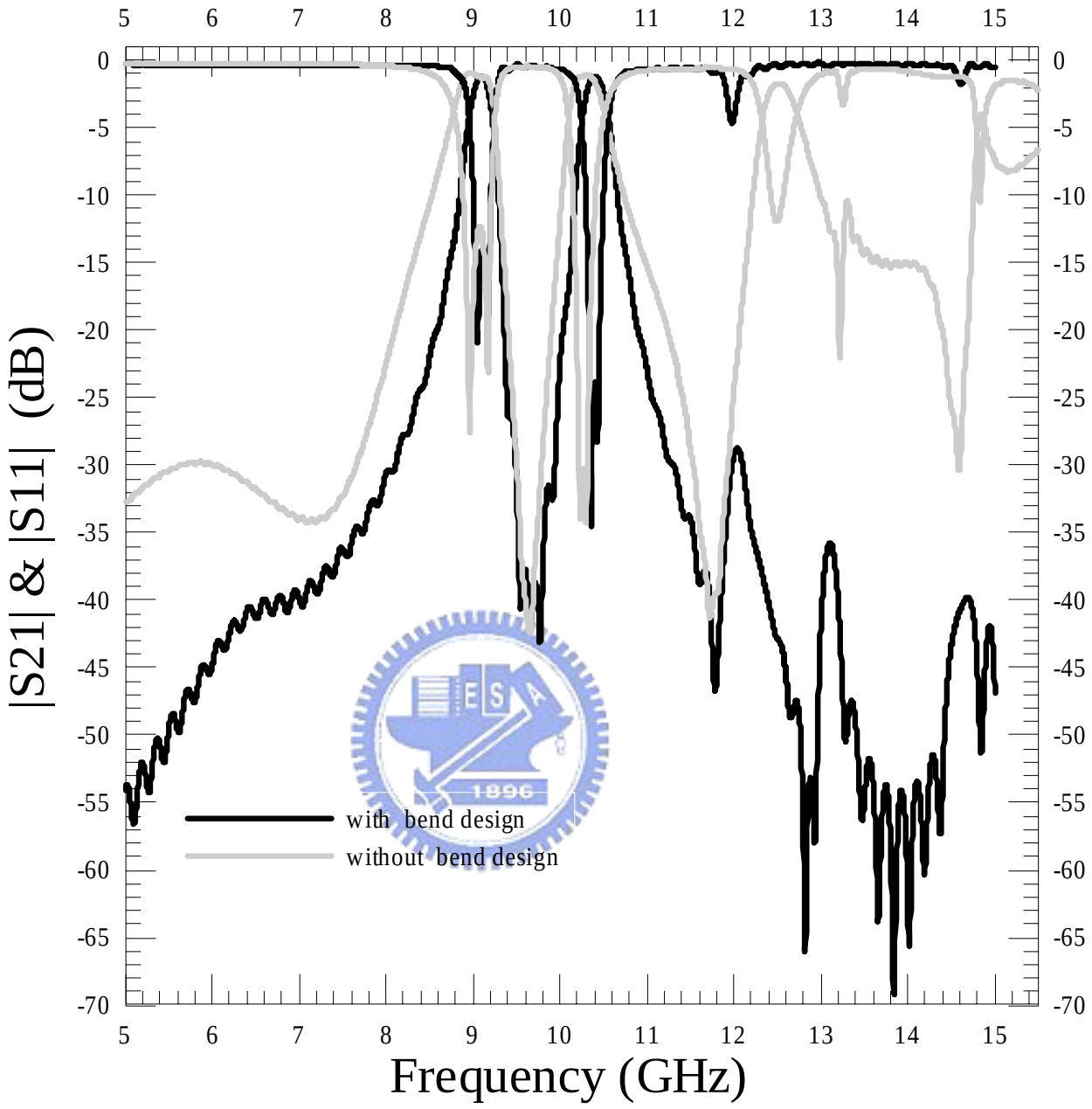

Figure 5. Simulated results by comparing the two filters with different the input/output design structures

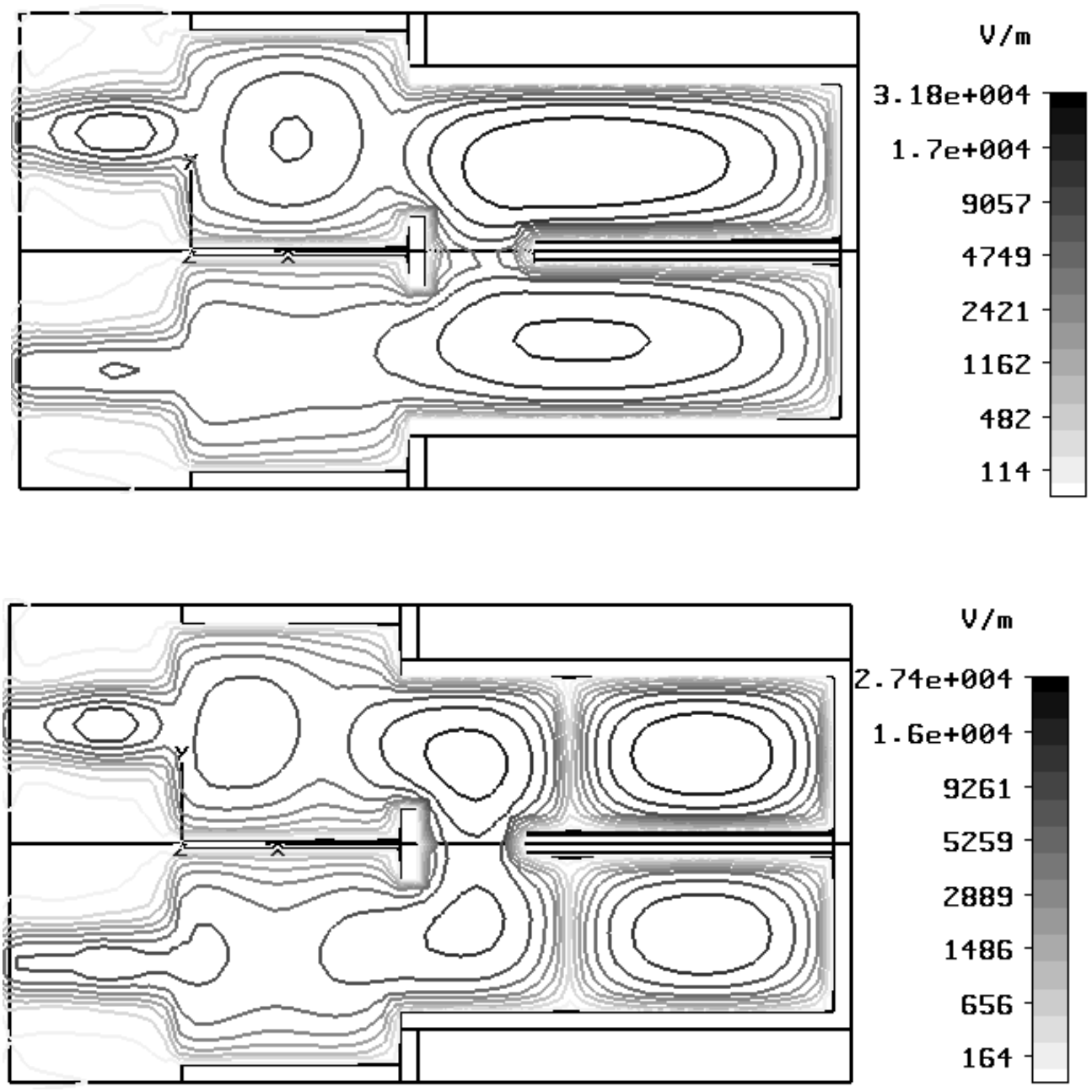

Figure 6. (a) Simulated electric field strength (E_z) distribution over each cavity at 9.1GHz and 10.2GHz

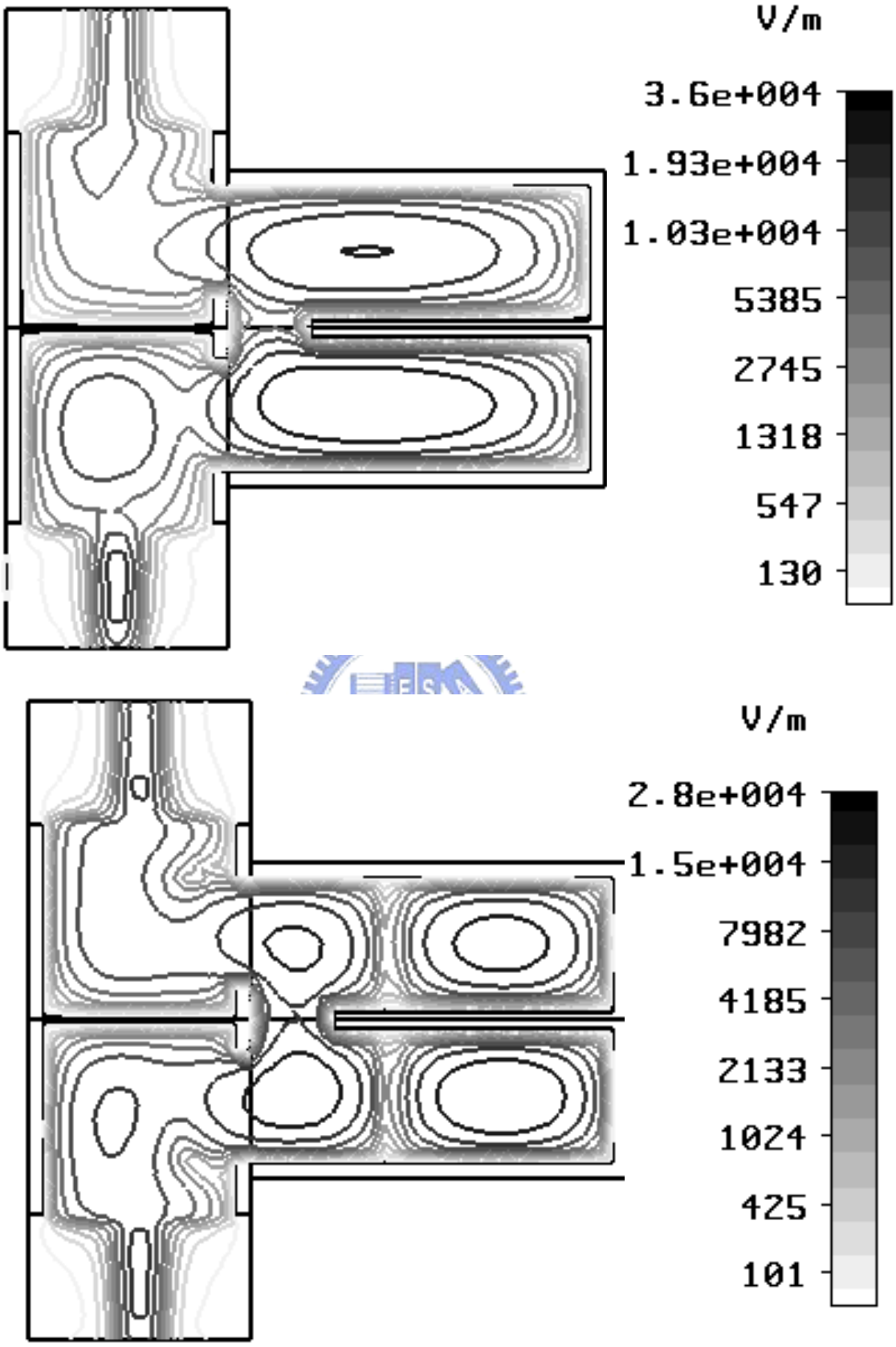

Figure 6. (b) Simulated electric field strength (E_z) distribution over each cavity at 9.1GHz and 10.2GHz

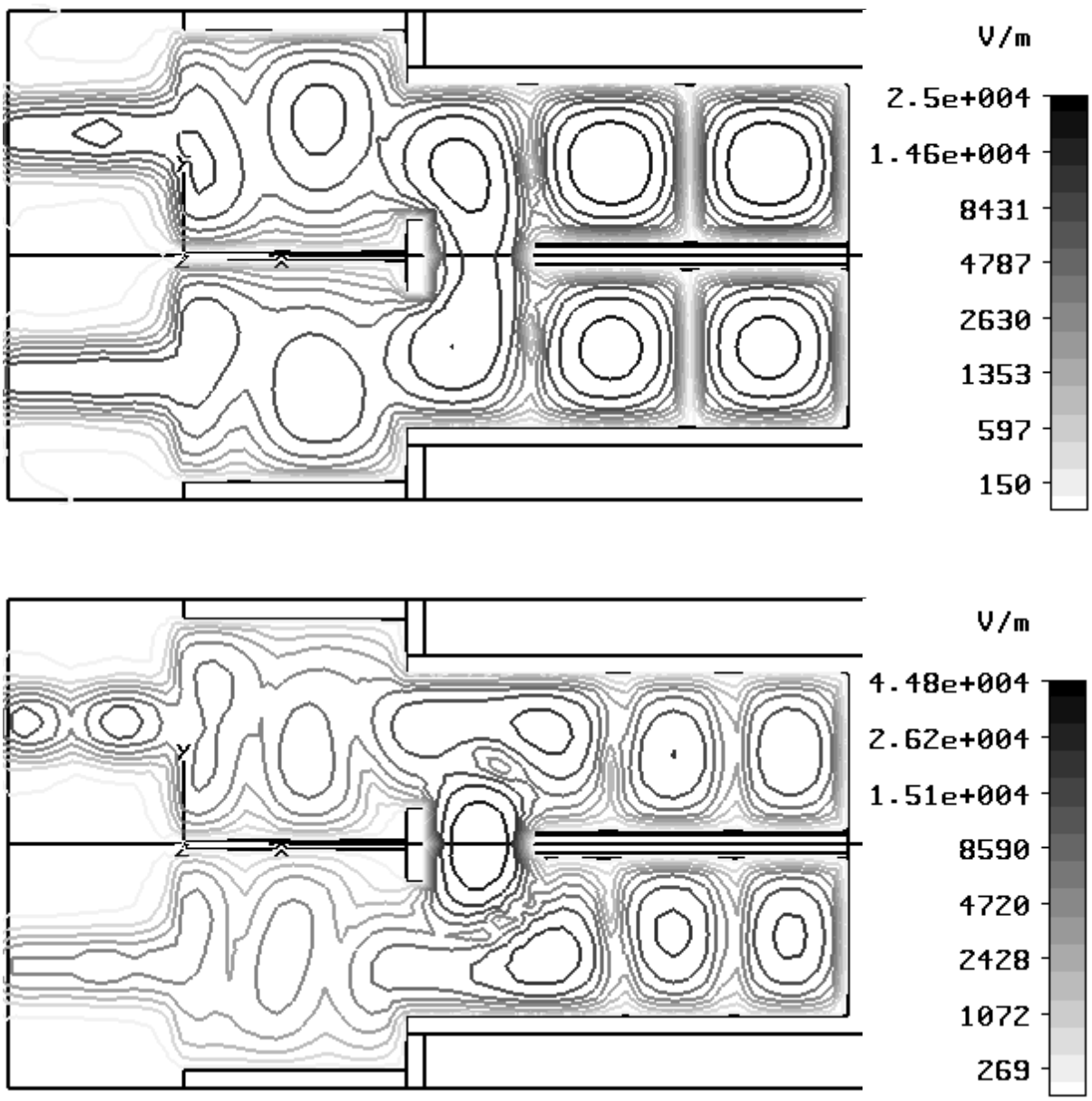

Figure 6. (c) Simulated electric field strength (E_z) distribution over each cavity at 12.4GHz and 14.7GHz

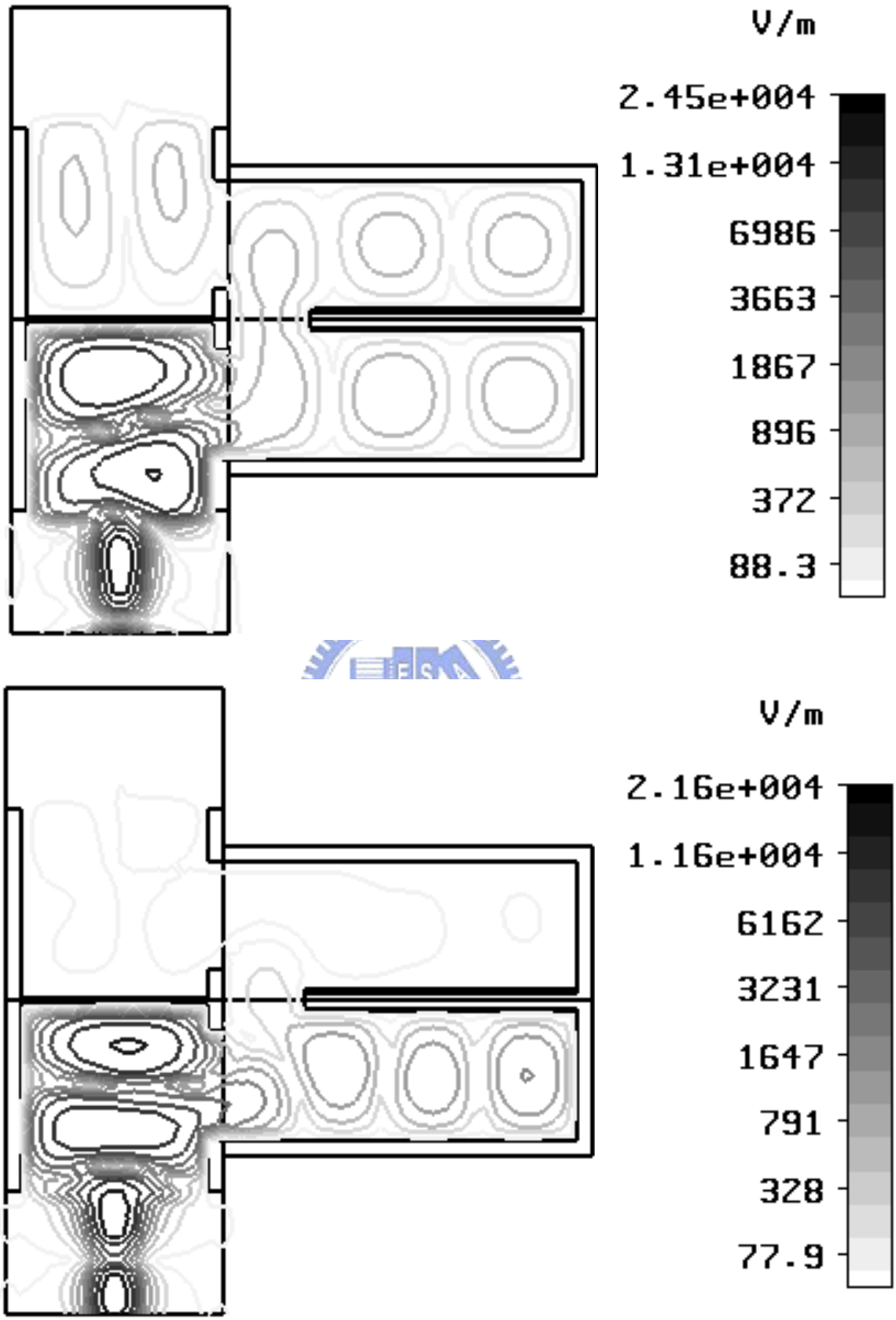

Figure 6. (d) Simulated electric field strength (E_z) distribution over each cavity at 12.4GHz and 14.7GHz

To verify the proposed concept, prototypes of the proposed filter structures were implemented and measured. The dual-bandpass filters are implemented on the microwave substrate RO4003 of thickness 0.508 mm, relative dielectric constant 3.82, and loss tangent 0.0027. First, the pattern of the transitions, the via-hole-arrays on the substrate, and the side walls of the PCB are processed by mechanical carving and followed via-hole arrays by copper plating technique to connect the top and bottom metal surfaces to realize the rectangular waveguide. The metallic vias have the diameter of 0.5 mm and 1 mm, respectively, and the pitch between two adjacent vias is from 0.5 mm to 1.2 mm. An HP 8722D network analyzer was used for the measurements, and the experimental results are performed in the frequency range from 5 to 15 GHz. Besides, for every simulated results, including the insertion loss and return loss, the full-wave analysis is conducted by using CST Microwave Studio 5.0, based on the Finite Integration Technique (FIT) which is first proposed by Weiland.

3-1 **Simulated and measured results of the dual-bandpass filter with adjustable second-passband**

In this section, we will implemented the four filters with different cavity lengths to demonstrate that the central frequency of the second pass band is tunable. Each the dual-bandpass filters is designed in X-band. Besides, we can observe that the proposed filter is capable of suppressing the higher mode response at high band from the measured results.

First, we will start by considering the filter with cavity length of 20 mm, and the measured results of this filter will be given below. Figure 7 shows the photograph of the dual-bandpass filter and the designed parameters are listed in Table 1.

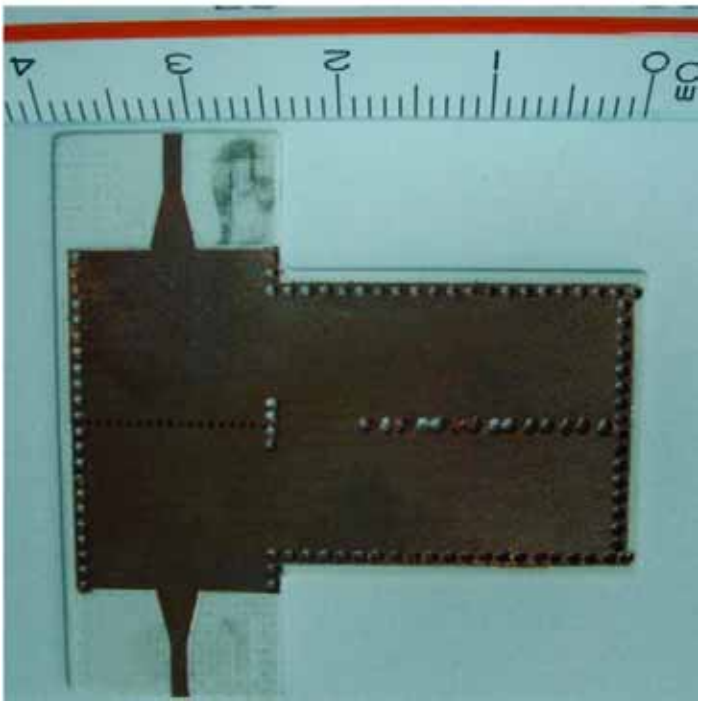

Figure 7. The photograph of the implemented dual-bandpass filter

radius of big via hole：d_1	1 mm
radius of small via hole：d_2	0.5 mm
width of waveguide：w_x	12.6 mm
width of cavity：w_y	9.4 mm
input/output waveguide length：l_y	20 mm
l_{y1}	4.5 mm
input/output cavity length：l_{y2}	6.5 mm
l_{y3}	2 mm
length of cavity：l_x	38 mm
width of aperture：w_a	6 mm
Micro-strip line width ：m_w	1.175 mm
Micro-strip line length ：m_l	4 mm
Taper transition width：t_w	2.6 mm
Taper transition length：t_l	3.3 mm

Table 1.: structure parameter

The measured results, shown in figure 8, indicates that the pass band of the dual-bandpass filter are at respective frequencies of 9.17 GHz and 10.35 GHz. The solid and dashed lines represent the measured and simulated results. In the low-band at 9.17 GHz, the insertion loss is − 2.34 dB and the return loss is < 11 dB. In the high-band at 10.35 GHz , the insertion loss is − 2.54 dB and the return loss is < 15 dB. The 3-dB fractional bandwidth of the low-band is 3.4%, and the 3-dB fractional bandwidth of the high-band is 2.67%. The Q factor of the low-band is 269, and the Q factor of the high-band is 387. Between these two pass band, a transmission zero at 9.82 GHz is clearly observed, which gives 65 dB rejection. As can be seen, the measured results agree with the simulated data.

In many microwave communications systems, the group delay is an important measurement

parameter because the phase response in the pass band is affected by the group delay. Therefore, we also presented the measured results of the group delay at respective pass band in Figure 9. The variation of the group delay of S21 is 0.4ns at the first pass-band. The variation of the group delay of S21 is 0.2ns at the second pass-band.

Finally, it is interesting to observe the higher mode responses of this filter at high bend. Due to the bend design, the higher harmonics responses did not appear. It is obvious that the out-of-band rejections of the filter is at least more than 25 dB over the measured frequency range, resulted in good stopband response.

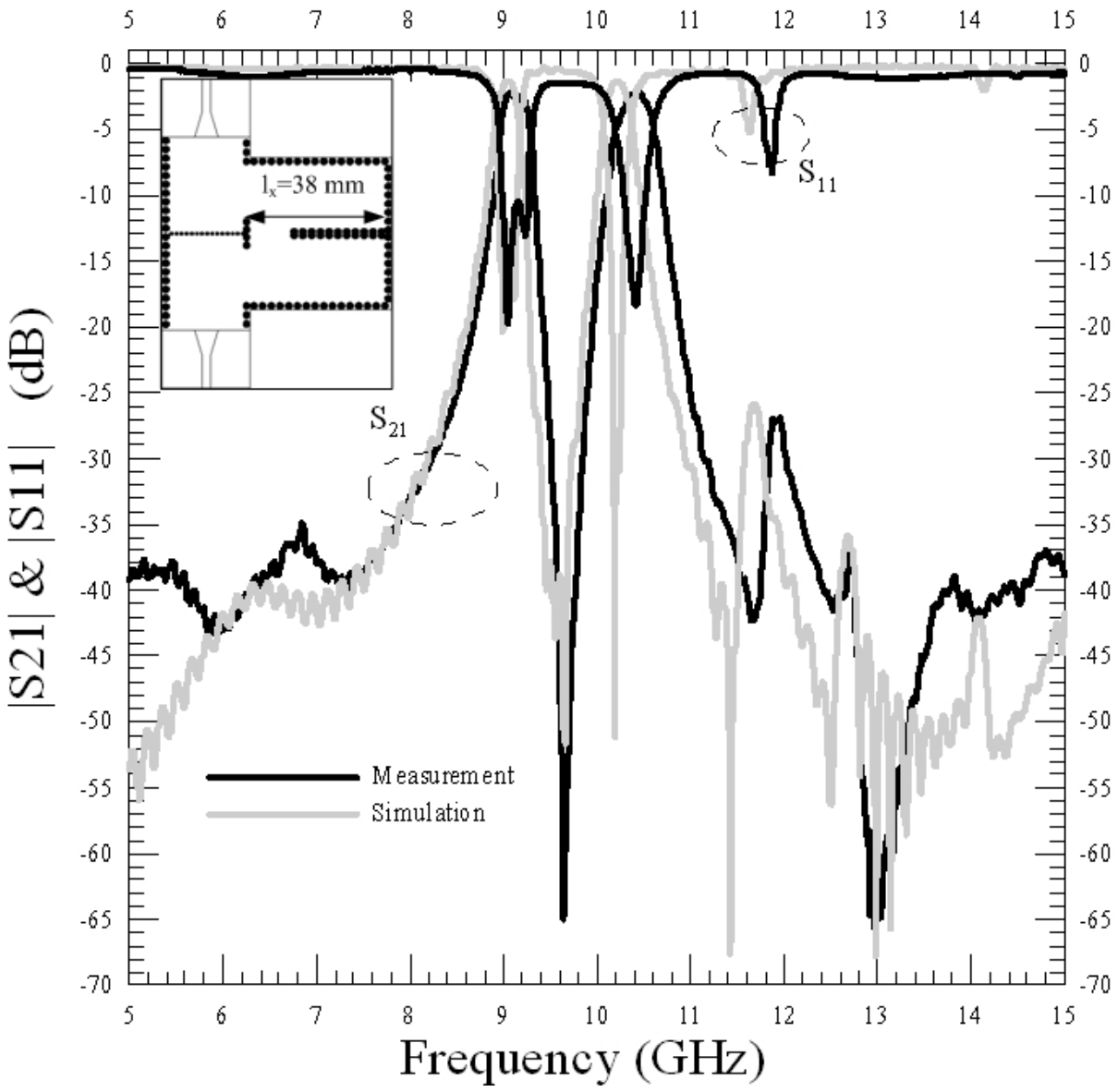

Figure 8. Simulated and measured results of the dual-bandpass filter

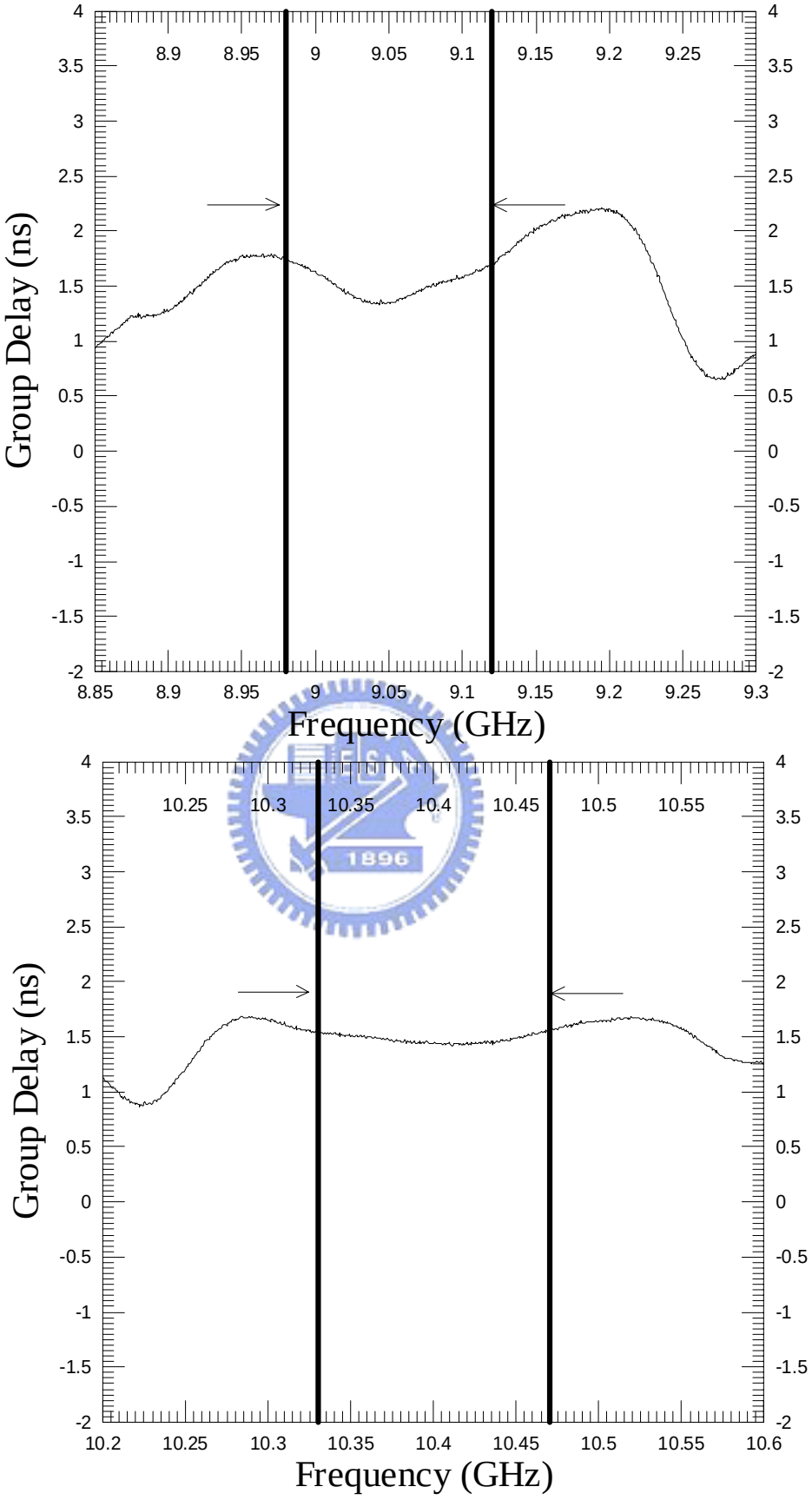

Figure 9. Measured results of the dual-bandpass SIW filter

The second dual-bandpass filter uses a cavity length l_x=36mm. The designed parameters of this filter are listed in Table 2. The measured and simulated results of the dual-bandpass filter, including the group delay, are shown in figure 10 and figure 11. The variation of the group delay of S21 is 0.2ns at the first pass-band. The variation of the group delay of S21 is 0.3ns at the second pass-band.

radius of big via hole：d_1	1 mm
radius of small via hole：d_2	0.5 mm
width of waveguide：w_x	12.2 mm
width of cavity：w_y	9.4 mm
input/output waveguide length：l_y	20 mm
l_{y1}	4.5 mm
input/output cavity length：l_{y2}	6.5 mm
l_{y3}	2 mm
length of cavity：l_x	36 mm
width of aperture：w_a	6 mm
Micro-strip line width ：m_w	1.175 mm
Micro-strip line length ：m_l	5 mm
Taper transition width：t_w	4.6 mm
Taper transition length：t_l	2.3 mm

Table 2.: structure parameter

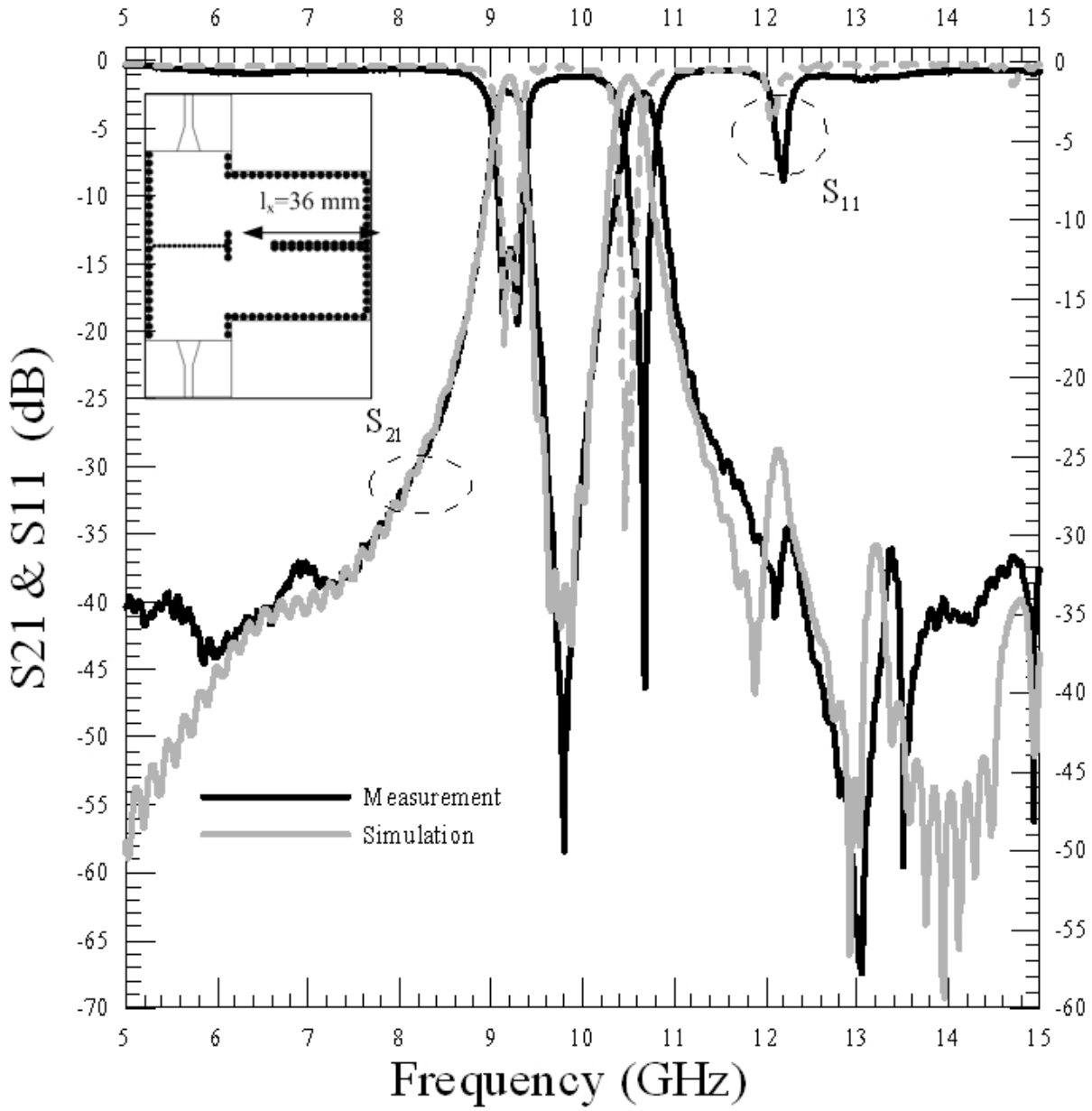

Figure 10. Simulated and measured results of the second dual-bandpass filter

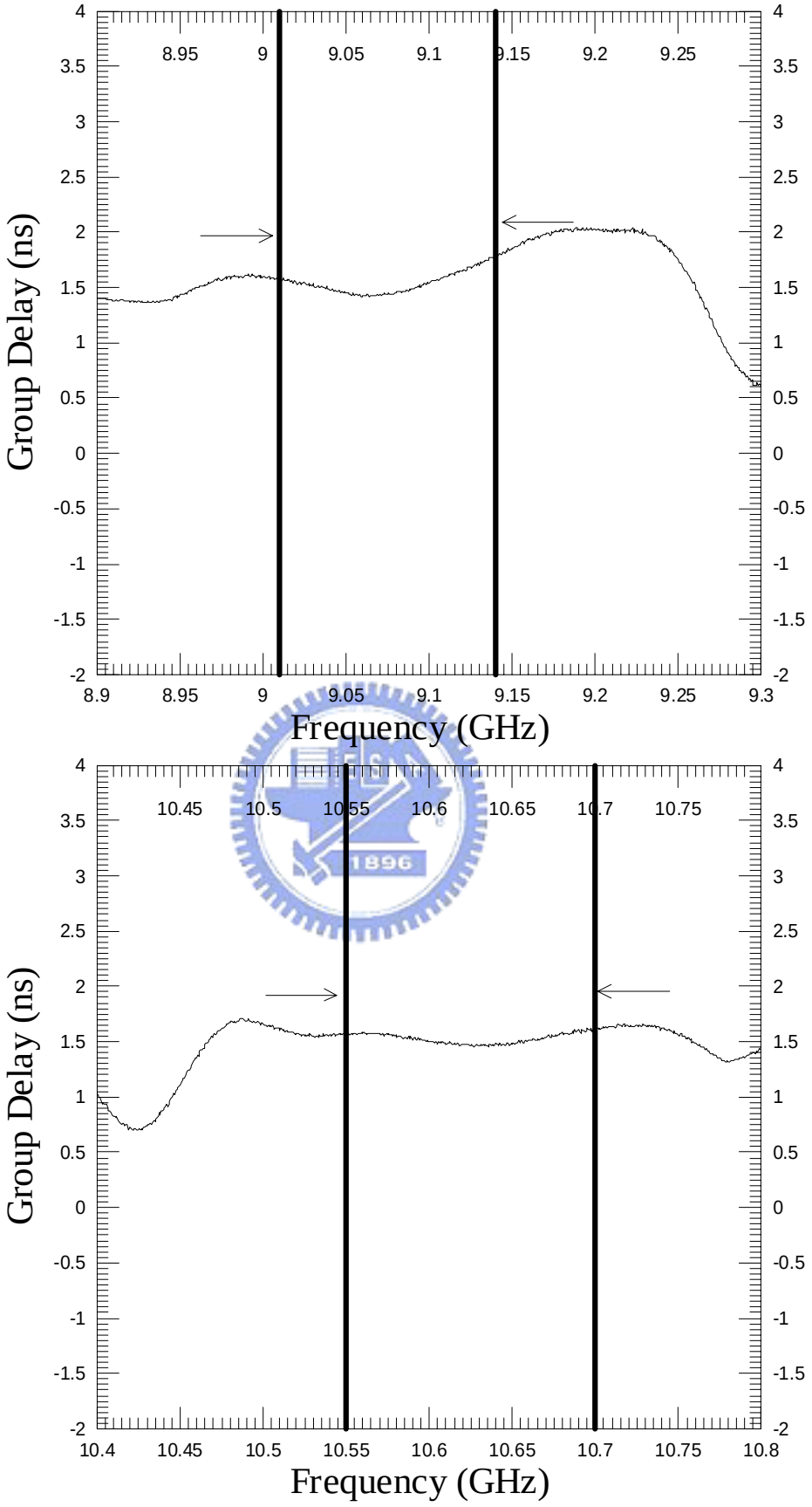

Figure 11. Measured results of the dual-bandpass filter

The second dual-bandpass filter specifications are the follows:

Design	Low-band (GHz)	Q factor	3-dB fractional bandwidth (%)	High-band (GHz)	Q factor	3-dB fractional bandwidth (%)
Measurement	9.23	279	3.33	10.67	330	3.23
Simulation	9.2	288	3.19	10.52	333	3.15

In the low-band at 9.23 GHz ,the insertion loss is − 2.43 dB and the return loss is < 13.5 dB. In the high-band at 10.56 GHz, the insertion loss is − 2.64 dB and the return loss is higher than 20 dB. It is obvious that the out-of-band rejections of the filter is at least more than 35 dB over the measured frequency rang.

Next, the cavity length of the dual-bandpass filter is designed as 34 mm. The designed parameters of this filter are listed in Table 3. The measured and simulated results of the dual-bandpass filter, including the group delay, are shown in figure 12 and figure 13. The variation of the group delay of S21 is 0.2ns at the first pass-band. The variation of the group delay of S21 is 0.3ns at the second pass-band.

radius of big via hole：d_1	1 mm
radius of small via hole：d_2	0.5 mm
width of waveguide：w_x	12.0 mm
width of cavity：w_y	8.3 mm
input/output waveguide length：l_y	13.5 mm
l_{y1}	4.5 mm
input/output cavity length：l_{y2}	6.5 mm
l_{y3}	2 mm
length of cavity：l_x	34 mm
width of aperture：w_a	6 mm
Micro-strip line width ：m_w	1.175 mm
Micro-strip line length ：m_l	4.67 mm
Taper transition width：t_w	3.46 mm
Taper transition length：t_l	3.3 mm

Table 3: structure parameter

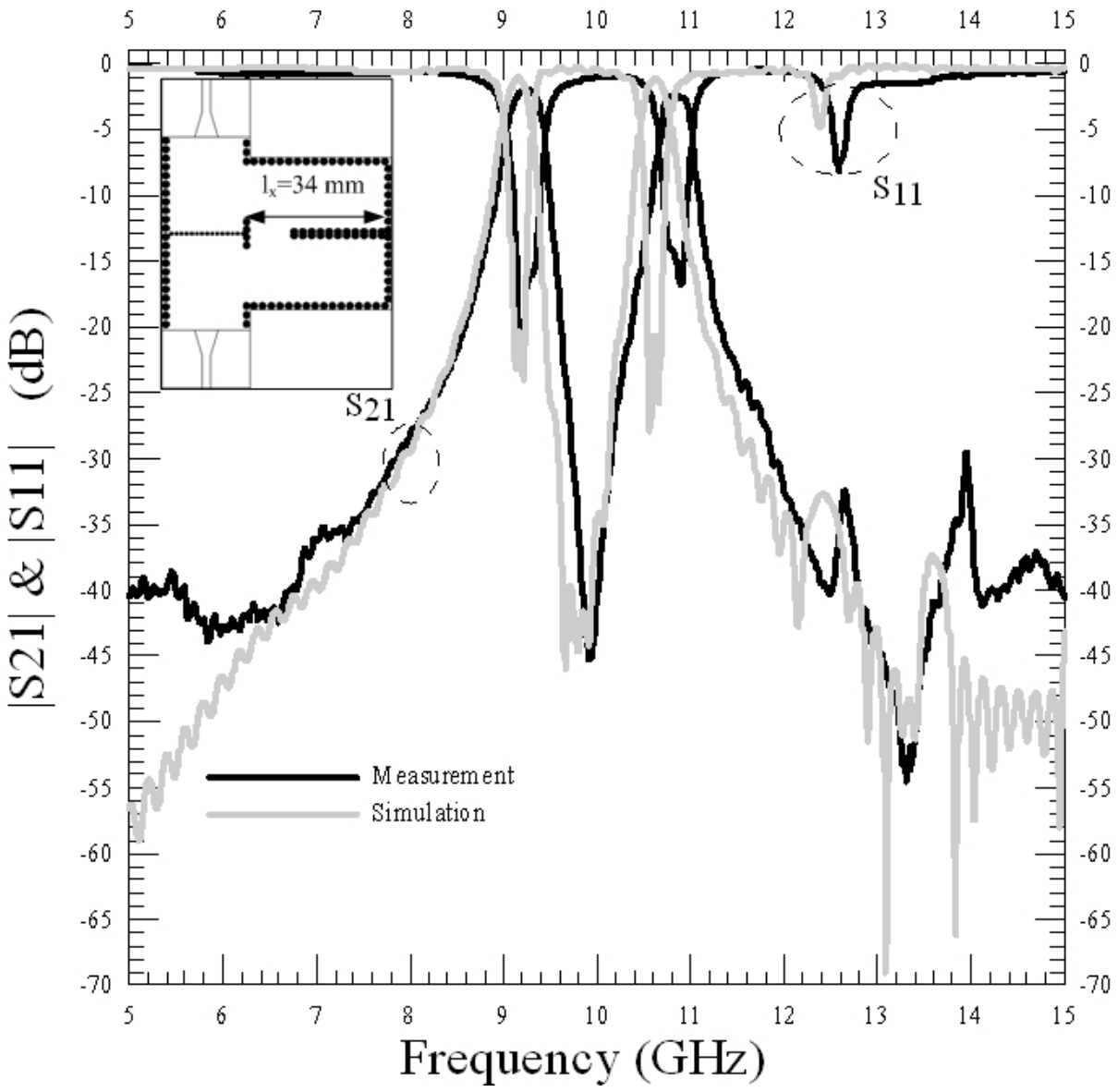

Figure 12. Simulated and measured results of the second dual-bandpass filter

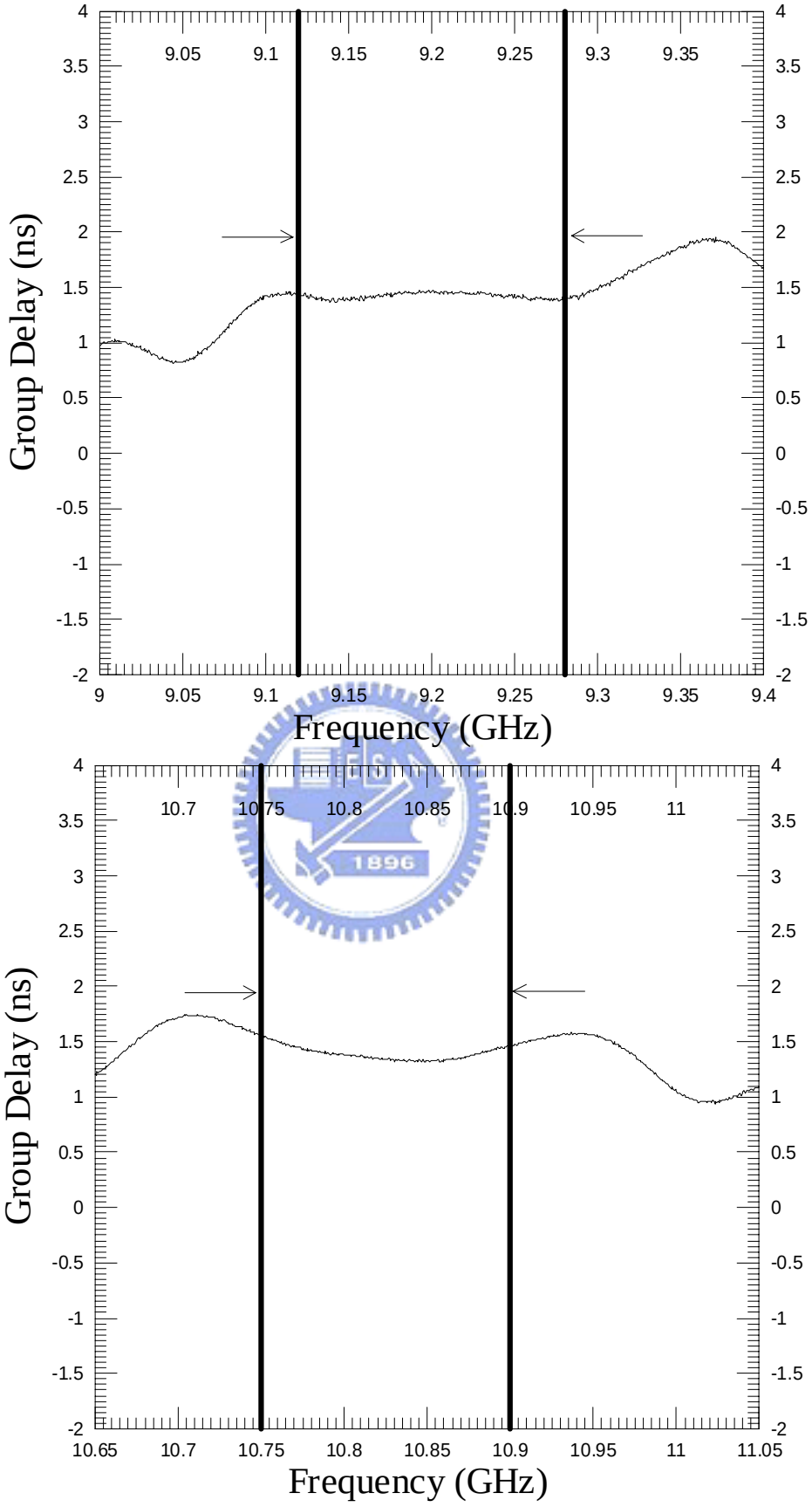

Figure 13. Measured results of the dual-bandpass filter

The third dual-bandpass filter specifications are the follows:

Design	Low-band (GHz)	Q factor	3-dB fractional bandwidth (%)	High-band (GHz)	Q factor	3-dB fractional bandwidth (%)
Measurement	9.25	218	4.24	10.9	316	3.44
Simulation	9.24	228	4.04	10.82	325	3.32

In the low-band at 9.25 GHz ,the insertion loss is − 2.73 dB and the return loss is higher than 15.5 dB. In the high-band at 10.9 GHz, the insertion loss is − 2.84 dB and the return loss is higher than 15 dB. It is obvious that the out-of-band rejections of the filter is at least more than 30 dB over the measured frequency rang.

Finally, the fourth dual-bandpass filter with cavity length of 32 mm filter is designed. The designed parameters of this filter are listed in Table 4. The measured and simulated results of the dual-bandpass filter, including the group delay, are shown in figure 14 and figure 15. The variation of the group delay of S21 is 0.5ns at the first pass-band. The variation of the group delay of S21 is 0.2ns at the second pass-band.

radius of big via hole：d_1	1 mm
radius of small via hole：d_2	0.5 mm
width of waveguide：w_x	11.6 mm
width of cavity：w_y	8.85 mm
input/output waveguide length：l_y	13.5 mm
l_{y1}	4.5 mm
input/output cavity length：l_{y2}	6.5 mm
l_{y3}	2 mm
length of cavity：l_x	32 mm
width of aperture：w_a	6 mm
Micro-strip line width ：m_w	1.175 mm
Micro-strip line length ：m_l	5.67 mm
Taper transition width：t_w	3.46 mm
Taper transition length：t_l	3.0 mm

Table 4 : structure parameter

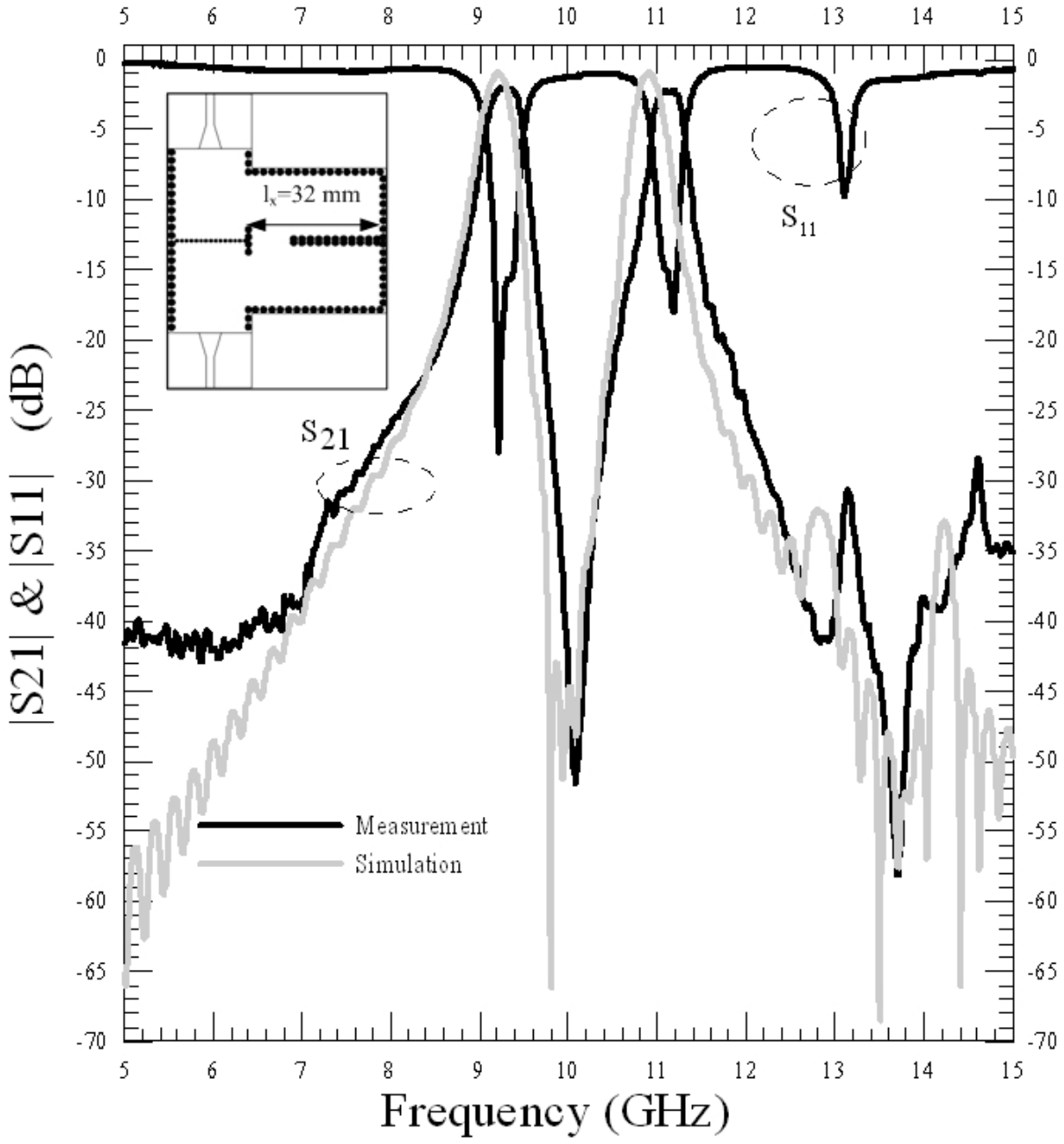

Figure 14. Simulated and measured results of the second dual-bandpass filter

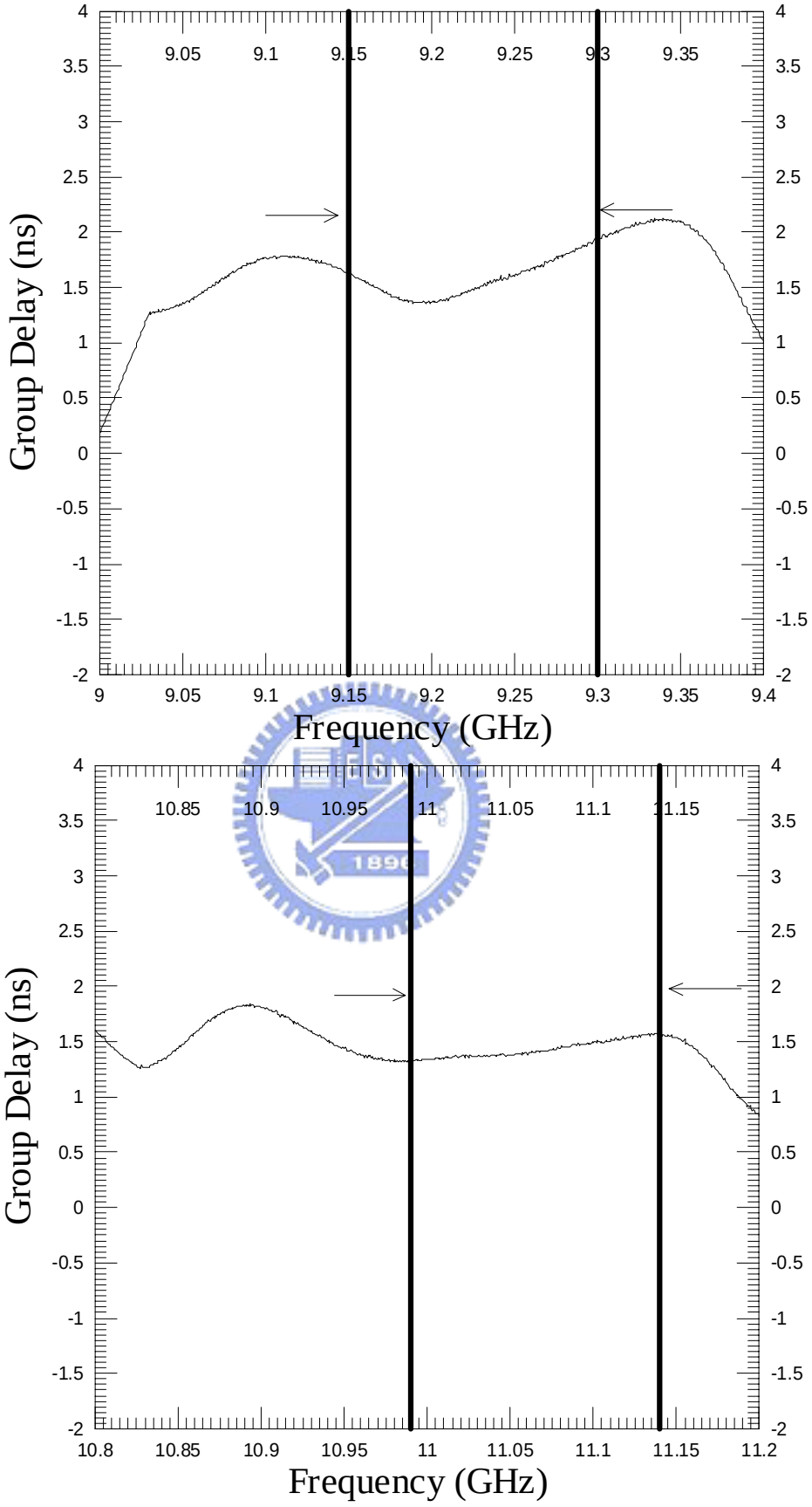

Figure 15. Measured results of the dual-bandpass filter

The four dual-bandpass filter specifications are the follows:

Design	Low-band (GHz)	Q factor	3-dB fractional bandwidth (%)	High-band (GHz)	Q factor	3-dB fractional bandwidth (%)
Measurement	9.26	194	4.75	11.07	284	3.89
Simulation	9.24	203	4.55	10.95	292	3.74

In the low-band at 9.26 GHz, the insertion loss is − 2.78 dB and the return loss is higher than 15.5 dB. In the high-band at 11.07 GHz, the insertion loss is − 2.87 dB and the return loss is higher than 15 dB. It is obvious that the out-of-band rejections of the filter is at least more than 28 dB over the measured frequency rang.

So far, we have simulated, fabricated, and measured the four filters with different cavity lengths and the characteristics of each filter are presented in detail. Finally, all the simulated and measured result of each filter are shown in figure 16. It will be clear from this figure 16 that the central frequency of the second pass-band is tunable by means of appropriately changing the cavity length. Furthermore, specifications of each filter are not altered by the movement of the second pass band such as bandwidth. Besides, we can see from the simulated results, shown in figure 17, that the maximum tunable range of the second pass band is from 10 GHz to 11.8 GHz; meanwhile, the rejections at high band are at least more than 25 dB.

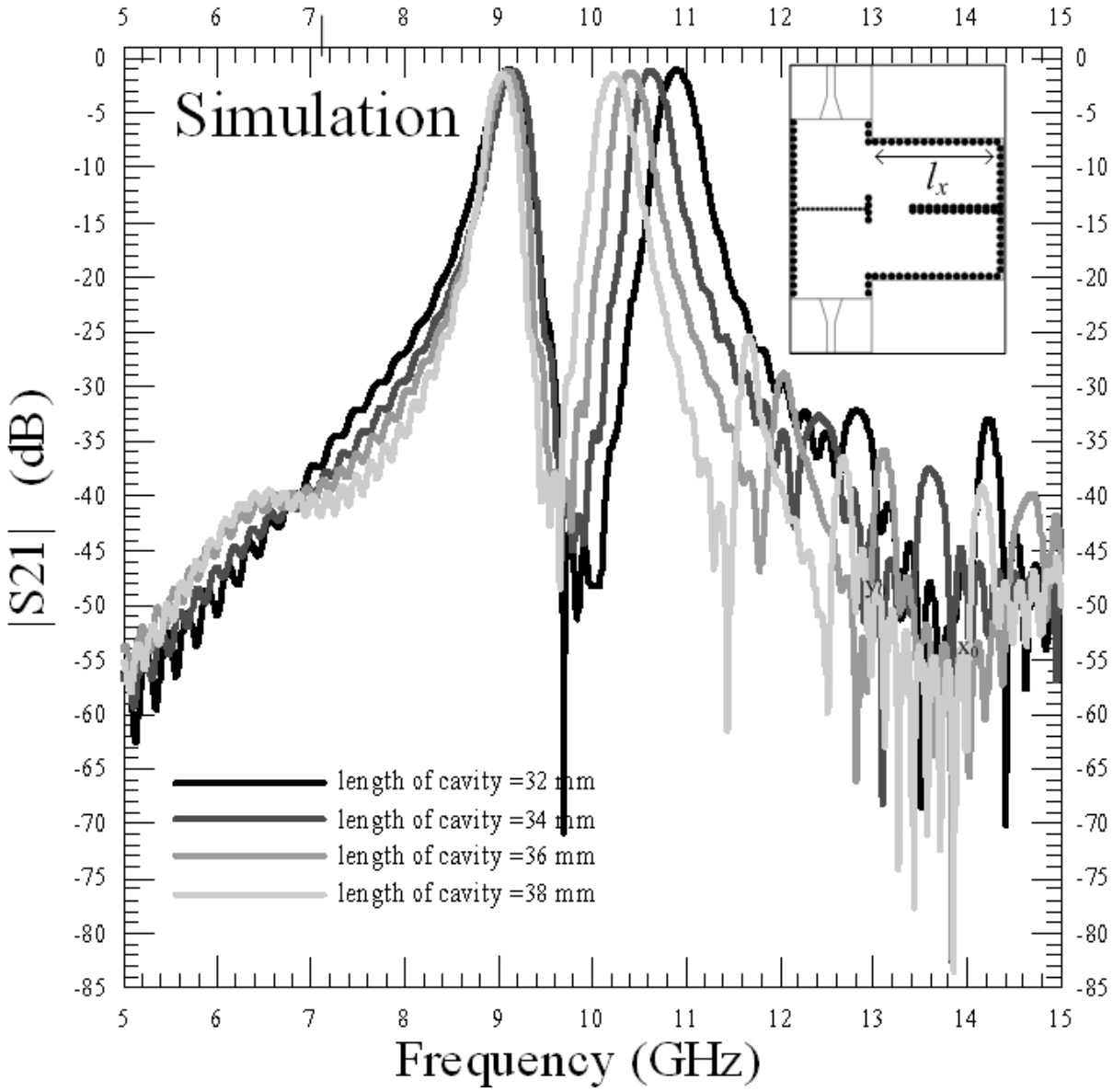
Simulation
|S21| (dB)
Frequency (GHz)
length of cavity =32 mm
length of cavity =34 mm
length of cavity =36 mm
length of cavity =38 mm
l_x
y
x0

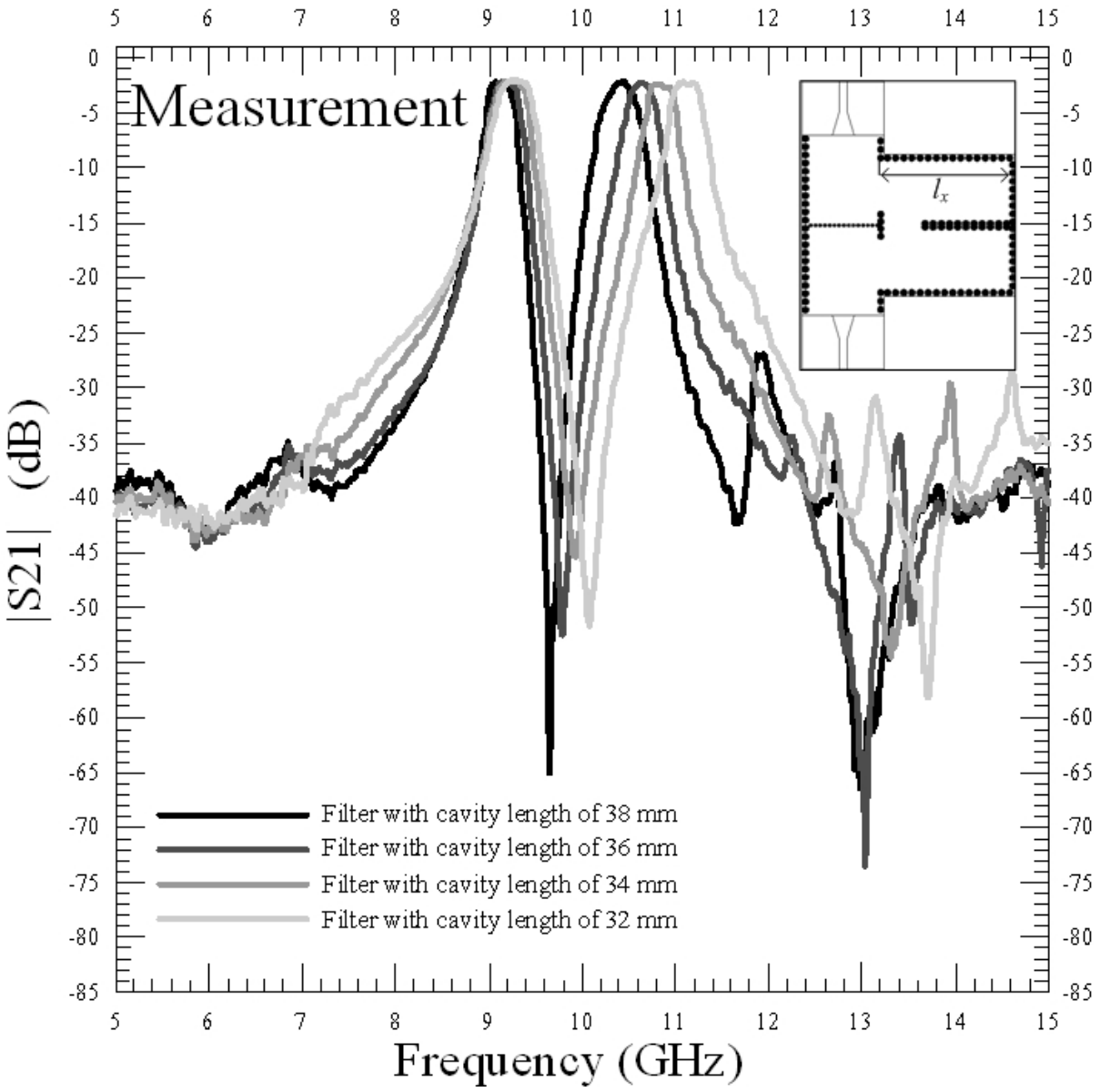

Figure 16. Simulated and measured results of the four dual-bandpass SIW filters with controllable the second pass-band

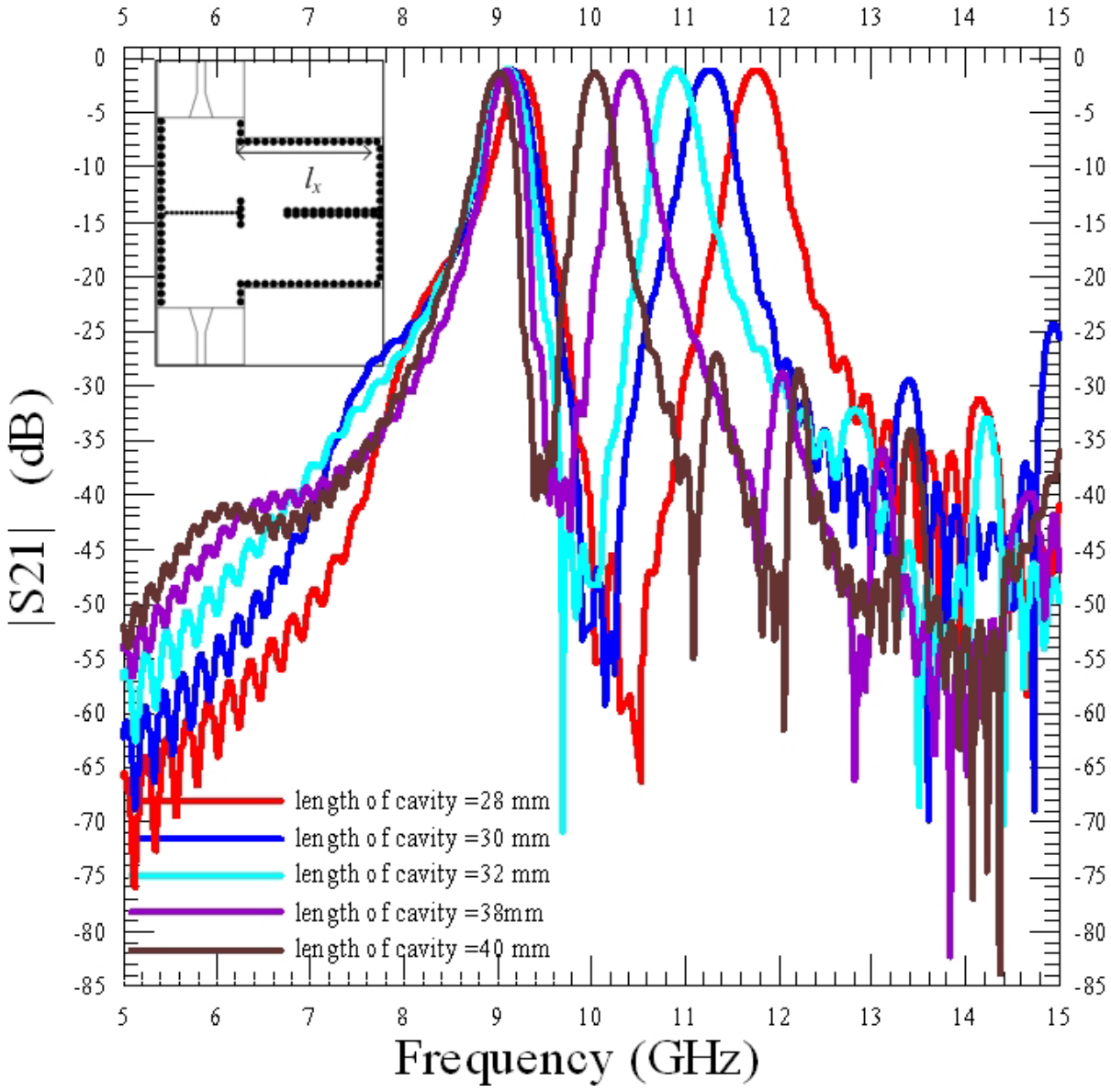

Figure 17. Simulated results of the five dual-bandpasds SIW filters with controllable the second pass-band

3-2 **measured results of the dual-bandpass filter with controllable**

fractional bandwidths

This section mainly describes that the bandwidths of the dual-bandpass filter can be adjusted by changing the aperture width (w_a). The three dual-bandpass filters are fabricated to realize the different bandwidths, and their measured results are plotted in figure18 to demonstrate the different bandwidths at 6 GHz and 8 GHz. The bandwidths of the three cases plotted in figure18 are (a) FBW =2.45% at the first pass band and FBW =2.5% at the second passb and, (b) FBW =5.45% at the first pass band and FBW =4.6% at the second pass band, (c) FBW =10.05% at the first pass band and FBW =9.35% at the second pass band. It will be clear from this figure 18 that the bandwidth is increased as the aperture width is increased.

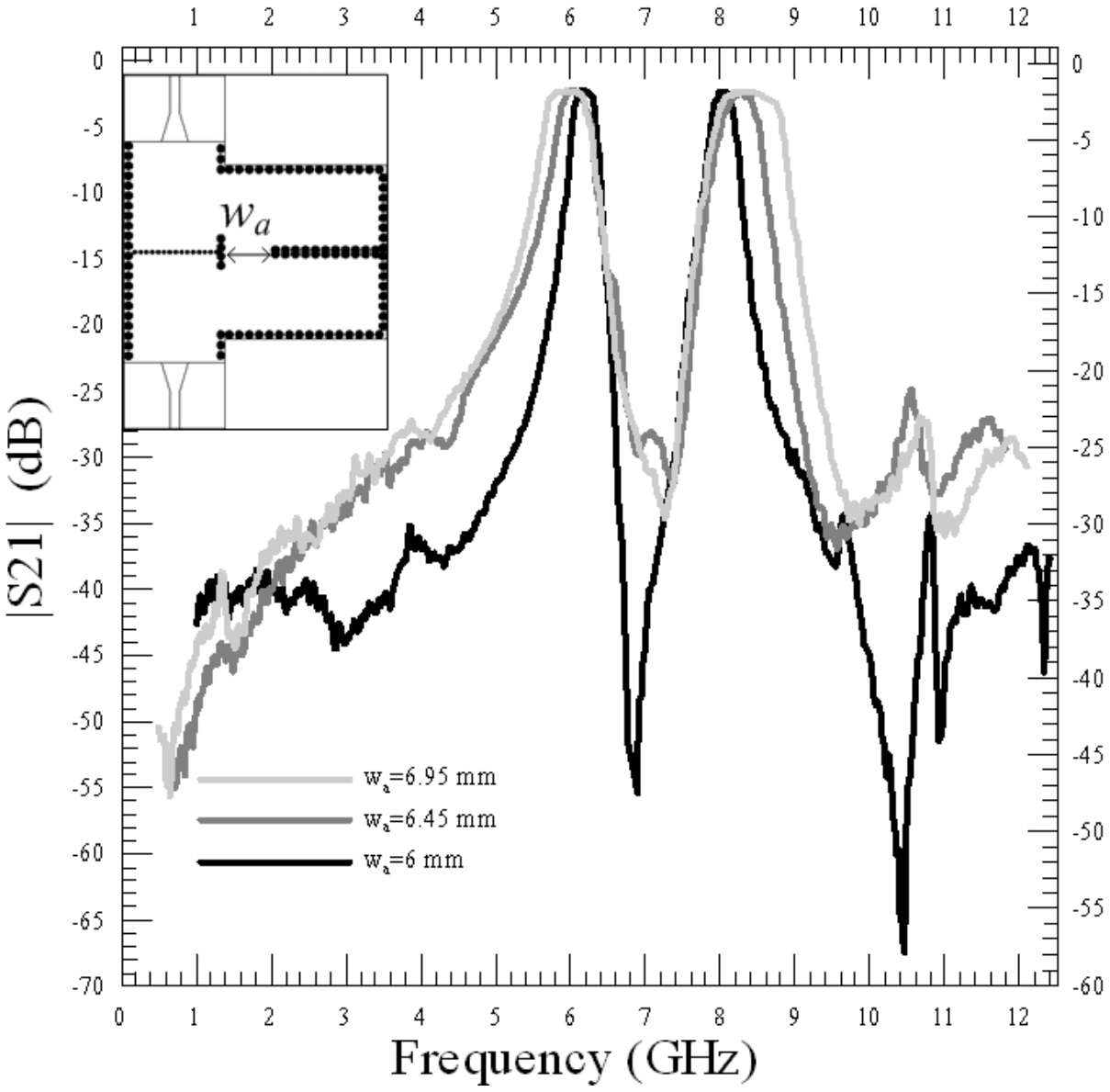

Figure 18. Measured results of the dual-bandpass SIW filters with varied width of aperture (w_a)

Chapter Ⅳ

Conclusion

The new proposed dual-bandpass filter has been developed in this thesis. The dual-bandpass filter with the capabilities of higher mode suppression are discussed and implemented by using the via-hole-wall technique. The proposed filter is easy to fabricate, and design. Because of the compact size, this proposed dual-bandpass filter is potentially suitable for implementation in the dual mode communication system, such as GSM and CDMA.

Bibliography

[1] B. N. Das, K. V. S. V. R. Prasad, and K. V. Seshagiri Rao, "Excitationof waveguide by stripline and microstrip-line-fed slots," *IEEE Trans.Microwave Theory Tech.*, vol. MTT-34, pp. 321–327, Mar. 1986.

[2] W. Grabherr, B. Huder, and W. Menzel, "Microstrip to waveguide transition compatible with MM-wave integrated circuits," *IEEE Trans. Microwave Theory Tech.*, vol. 42, pp. 1842–1843, Sept. 1994.

[3] T. Q. Ho and Y. Shih, "Spectral-domain analysis of E-plane waveguide to microstrip transitions," *IEEE Trans. Microwave Theory Tech.*, vol. 37,pp. 388–392, Feb. 1989.

[4] L. J. Lavedan, "Design of waveguide-to-microstrip transitions specially suited to millimeter-wave applications," *Electron. Lett.*, vol. 13, Sept.1977.

[5] K.Wu, "Integration and interconnect techniques of planar and nonplanar structures for microwave and millimeter-wave circuits-current status and future trend," in *Proc. Asia–Pacific Microw. Conf.*, Taiwan, R.O.C., Dec.2001, pp. 411–416.

[6] D. Deslandes and K. Wu, "Single-substrate integration technique of planar circuits and waveguide filters," *IEEE Trans. Microw. Theory Tech.*, vol. 51, no. 2, pp. 593–596, Feb. 2003.

[7] S. Germain, D. Deslandes, and K. Wu, "Development of substrate integrated waveguide power dividers," in *Proc. Can. Electr. Comput. Eng. Conf.*, vol. 3, May 2003, pp. 1921–1924.

[9] Xiaoping Chen, Wei Hong, *E*, Tiejun Cui, Jixin Chen, and Ke Wu,"Substrate integrated waveguide (SIW) linear phase filter," *IEEE Trans. Microw. Theory Tech.*, , vol. 15, no. 11, Nov. 2005

[10]Y. L. Kuo and K. L. Wong, "Printed double-T monopole antenna for 2.4/5.2 GHz dual-band WLAN operations," *IEEE Trans. Antennas Propag.*, vol. 51, no. 9, pp. 2187–2192, Sep. 2003.

[11]H. Hashemi and A. Hajimiri, "Concurrent multiband low-noise amplifiers theory, design

and applications,” *IEEE Trans. Microw. Theory Tech.*, vol. 50, no. 1, pp. 288–301, Jan. 2002.

[12] H. Miyake, S. Kitazawa, T. Ishizaki, T. Yamada, and Y. Nagatomi, “A miniaturized monolithic dual band filter using ceramic lamination technique for dual mode portable telephones,” in *IEEE MTT-S Int. Dig.*,1997, pp. 789–792.

[13]S. F. Chang, Y. H. Jeng, and J. L. Chen, “Dual-band step-impedance bandpass filter for multimode wireless LANs,” *Electron. Lett.*, vol. 40, pp. 38–39, Jan. 2004.

[14]L. C. Tsai and C. W. Hsue, “Dual-band bandpass filters using equal length coupled serial-shunted lines and Z-transform technique,” *IEEE Trans. Microw. Theory Tech.*, vol. 52, no. 4, pp. 1111–1117, Apr. 2004.

[15]H. Miyake, S. Kitazawa, T. Ishizaki, T. Yamada, and Y. Nagatomi, “A miniaturized monolithic dual band filter using ceramic lamination technique for dual mode portable telephones,” in *IEEE MTT-S Int. Dig.*,1997, pp. 789–792.

[16]D. Deslandes, and K. Wu, "Integrated microstrip andrectangular waveguide in planar form," *IEEE Microwaveand Guided Wave Letters,* vol. 11, no. **2,** pp.